Self-Assembly Synthesis and Electrochemical Performance of Partially Reduced Graphene Oxide Supported Hierarchical MnO_2 Nanonocomposite for Supercapacitor

Muhammad Ishaq, Maher Jabeen, and Weiming Song*
College of Chemistry and Chemical Engineering, Qiqihar University, Qiqihar Heilongjiang 161006, P.R. China.
qdsongweiming@163.com*

(Received on 27th March 2018, accepted in revised form 22nd November 2018)

Summary: Partially reduced graphene oxide supported hierarchical birnessite-type manganese oxide (MnO_2) nanonocomposite (MnO_2-pGO) with large surface area (116 m^2 g^{-1}) were successfully synthesized by a facile ultrahigh dilute vesicle solution approach, via surfactant Hexadecyltrimethylammonium bromide (CTAB) and sodium dodecylbenzenesulfonate (SDBS), as a structure-directing agent. The resultant structure exhibit hierarchical porous MnO_2 nanocluster, which were self-assembled from elongated nanorods and grafted successfully on the surface of the pGO nanosheets. Furthermore, the obtained MnO_2-pGO nanocomposite was found to exhibit favorable electrochemical activity showing ultra-high specific capacitance of (282 F/g at 0.5 A/g), the enhanced rate capability of (67.7%) at 10 A/g), the most stable capacitance retention (91.4 %of its initial capacitance was retains after 5000 cycles, with ~100% Coulombic efficiency). The result suggests that the approach is not only effective to deposit MnO_2 over the pGO sheets, but also offered great promise to prepare other pGO- metal oxide composite electrode materials for supercapacitor.

Keywords: MnO_2, pGO, Vesicle solution, Supercapacitors.

Introduction

Recently, energy storage and conversion technology has become a fundamental research and development center, because of fossil fuels depletion and incredible serious environmental issues caused by their combustion [1]. The growing need of electronic devices has led researchers to focus on novel and smart electrochemical material designs having unique properties of high redox capability, low-cost, and eco-friendliness [2]. To date, several effective configurations have been designed to construct electrochemical materials for supercapacitors [3]. Among which majorities are integrated by two-dimensional layered materials, including metal dichalcogenides (MoS_2, $MoSe_2$, and WS_2), [4, 5] electrically conducting polymers, [6] transition metal (Ni, Mn, Co, Fe, Ru) oxides/hydroxide and carbon-based graphene have attracted substantial attention because of pseudocapacitive behaviors as well as their high electrical properties across the electrode/electrolyte interface.[2, 7–13] Within this class, manganese dioxide (MnO_2), containing transition metal is considered as one kind of the most promising energy materials for pseudocapacitors [14, 15]. Nevertheless the electrochemical performances (ECP) of MnO_2 are often hampered by their relatively low electric conductivity, deprived mechanical stability and bad cycling stability [16].

To remedy the above limitations, Co-assembly of MnO_2 and carbon-based nanomaterial's, such as activated carbon, [17] carbon nanotubes, [18] carbon nanofibers, [19] and graphene, [20] have been used in constructing 2D/3D nanocomposite, which exhibits enhanced ECP. Among the various carbon-based materials, graphene and its chemical derivatives, aroused as potential substrates for assembling nanocomposite for energy-based applications, due to its superior electrochemical reactivity, high conductivity and exceptional electrode stability [21].Within this class, graphene oxide (GO) has revealed excessive coordinating potential with other materials to form GO based electrode material, due to the presence of oxygenic functional groups on the basal aromatic lattice [22, 23]. Nevertheless, GO undergoes poor electrical conductivity due to biased sp^3 hybridized geometry [24]. In contrast excellent conductivity is accomplished in case of reduced graphene oxide (RGO) with planar sp^2 hybridization, but this could happen by reducing the surface oxygen functional groups. Very recently, a new class of graphene derivative known as partially reduced graphene oxide (pGO) has materialized, wherein unlike reduced graphene oxide (RGO), pi-pi (π- π) conjugations are restored only partially. Thus, pGO hold the benefits of both GO and rGO at the same time.[25]

*To whom all correspondence should be addressed.

Yan *et al* [26]. Reported that the ECP of partially reduced graphene oxide nanosheet (prGON) are superior to that of the reduced graphene, owing to the remaining oxygen functional groups in prGON, facilitated the reactive sites for pseudocapacitance and enhance its capacitance and life time performance.

On the basis of the above considerations, in this work, partially reduced graphene oxide supported hierarchical birnessite-type manganese oxide (MnO_2) nanocomposite (MnO_2-pGO) were successfully synthesized by a facile ultrahigh dilute vesicle solution approach. Vesicles are usually spherical,(10 nm to 50 um diameter), enclosed and hollow lamellar aggregates with an arched bilayer membrane, consist of amphiphilic molecules, with an exclusive self-assembling properties and are widely explored as a template to synthesize novel nanostructured materials.[27,28] The structural and supercapacitive properties of the MnO_2-pGO nanpcomposite are briefly explored and discussed. In comparison, pure manganese oxide (MnO_2) was also fabricated by the same procedure. More importantly, the electrochemical studies of the MnO_2-pGO composite electrode exhibited significantly higher specific capacitance value (282 F/g), the better rate capability (67.7%) at 10 A/g), the most stable capacitance retention (98 %) after 5000 cycles, with ~100% Coulombic efficiency) and low R_{CT} value (2.032 Ω before and 2.733 Ω after 5000 charge discharge cycles from impedance measurements), making it the most favorable to be used an electrode energy materials for supercapacitor applications.

Experimental

Chemicals

Crude flake graphite powder (45 µm, 99 %), sulfuric acid (H_2SO_4, 98.08%), sodium nitrate ($NaNO_3$), potassium permanganate ($KMnO_4$), hydrogen peroxide (H_2O_2 30%), hexadecyl trimethyl ammonium bromide (CTAB), sodium dodecyl benzene sulfonate (SDBS), ascorbic acid, manganese(II) sulfate monohydrate ($MnSO_4.H_2O$, 99%) , and hydrochloric acid (HCL 36 %), were obtained from Tianjin Kemiou Chemical Reagent Co., Ltd. Water ultra-purified (UP) filtered resistivity (18.2 MΩ ·cm) were utilized throughout the experimentation.

Synthesis of pGO

Graphite oxide (GrO) was prepared from crude flake graphite by modified Hummers method.[29,30] pGO was prepared from the as-prepared GrO in the following typical process. First, 0.075g of GO was added into 75 ml of ultrapure water (1mg/ml) followed by 0.5 h of sonication. Then, 0.15g of ascorbic acid was added into the exfoliated graphene oxide suspension followed by another 10 min of stirring. The GO suspension was than refluxed in sonics ultrasonic processor at 90ºC (750 W, 20 kHz) with 40% amplitude for 0.5 h. Finally, the prepared pGO was washed using ultra-purified water through filtration.

Synthesis of MnO2-pGO nanocomposite

The MnO_2-pGO nanocomposite was synthesized through ultrahigh dilute vesicle solutions route as shown in **Error! Reference source not found.**. Typically, first CTAB and SDBS (1:2 molar ratios; 0.028 mol/L surfactant) aqueous solutions in twice-distilled water were prepared by weighting the surfactants and warming the dispersion to 40ºC for 24 h, respectively. Than a 6.5 mmol portion of $MnSO_4.H_2O$ and 3.8mmol of $KMnO_4$, were dissolved in 15 and 10 ml of UP water. Second, the as-prepared pGO was redispersed in 75 ml of the vesicle solution and was exfoliated via a Sonics ultrasonic processor (750 W, 20 kHz) with 40% amplitude for 1 h. Next the solution of $MnSO_4.H_2O$ and $KMnO_4$ were added drop wise into the GO-vesicle solution under stirring and the reaction was carried out at 45ºC for 12h. Finally the resultant dark-brown slurry of MnO_2-pGO were decanted and washed with UP water and ethanol to remove the organic compound prior to drying at 60 °C for 24 h in oven. For comparison, pure MnO_2 was fabricated in the absence of GO with the other same experimental condition, respectively.

Morphology and structural characterization

The phase purity of MnO_2-pGO and pure MnO_2 nanocomposite materials were analyzed using MAC Science MXP18 diffractometer. The Fourier transform infrared spectroscopy (FT-IR) measurement of the samples was recorded on Nicolet 6700 spectrophotometer. X-ray photoelectron spectroscopy (XPS) measurements were performed on Kratos Axis Ultra DLD instrument photoelectron spectroscope system. Scanning electron microscopy (SEM) and energy dispersive X-ray spectroscopy (EDS) images were acquired using a JEOL JSM-6360 electron microscope, Transmission electron microscopy (TEM) was performed on a FEI-TECHNI-G2 microscope. Raman spectra were run on an Ultra Resonance Raman spectroscopy (HORIBA Jobin Yvon S.A.S Lab RAM HR evo 800) with 32 nm line of an Ar ion laser as an excitation source. The Brunauer–Emmett–Teller (BET) specific surface area was measured using an automatic volumetric

sorption analyzer (Quantachrome, Autosorb-1, USA) apparatus.

Electrode fabrication and electrochemical characterization

Electrochemical characterizations were conducted in a three-electrode system on electrochemical analyzer (CHI660e, Shaanxi, China) at room temperature. A saturated calomel electrode (SCE), 1cm × 1cm platinum gauze and 1 M Na_2SO_4 aqueous solution were used as reference, counter electrodes and electrolyte, respectively. The working electrodes were fabricated by grinding mixing the obtained products, acetylene black as conductive material and poly(tertrafluoroethylene) (PTFE) as binder material with a mass ratio of 7.5:1:1. The mixture was dispersed in ethanol by ultrasonication for 15 minutes to form homogeneous slurry. The resultant slurry was coated onto the precleaned nickel foam current collector (1cm × 1cm). The electrode was than dried at 60 ˚C for 12 h in vacuum to evaporate solvent. Finally, the active materials coated nickel foam was pressed at 10 MPa for 10 min to obtain the working electrode. Cyclic voltammetry (CV) and galvanostatic charge/discharge experiment were studied in the optimized potential window of -0.1 to 0.9 V at various scan rate and current densities. Electrochemical impedance spectroscopy (EIS) was tested over the frequency range of 100 kHz to 0.01 Hz with an ac voltage of 5.0 mV. The specific capacitance C (F/g) was calculated from the discharge curves according to the following equations.[31]

$$Cs = I \times \Delta t / (\Delta V \times m) \qquad (1)$$

where I is the constant discharge current, Δt is the time of a discharge cycle, and ΔV is the potential drop during discharge[32], m is the mass of the active materials (g).

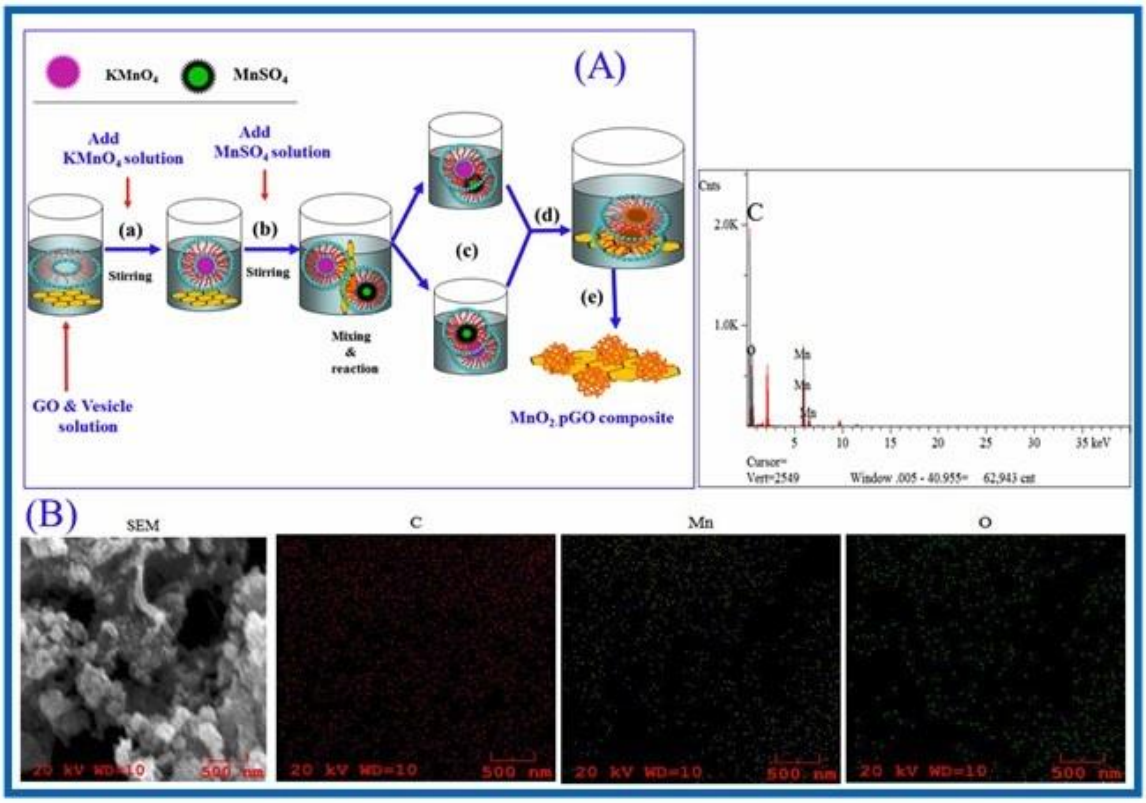

Fig. 1: (A) Schematic illustration of experimental steps for preparation of MnO_2-pGO composite via Vesicle solution reaction (a) Mixing process of $KMnO_4$ into GO and vesicle solution containing reactants; (b) mixing process of the $MnSO_4.H_2O$ solution (c) interfacial reaction; (d) nucleation and growth of MnO_2 in surfactant matrix after 12 h stirring period at 60°C ;(e) MnO_2-Graphene oxide composite powder after centrifugation, washing and freeze. (B) EDS mappings (C, O and Mn) and EDS spectrum for MnO_2-pGO nanocomposite

Results and Discussion

Physicochemical characterizations of materials

Fig 2 demonstrates XRD patterns of the samples. The most intensive sharp peak (001) centered at around 2θ = 10.7˚ (JCPDS card 75-1621) was observed, which is the characteristic reflection peak for GO, indicating an increase in interlayer d-spacing from 0.34 to 0.82 nm. This increase in the interlayer is caused by chemical oxidation and exfoliation of pristine graphite sheets. [33] The peaks seemed in the pattern of pure MnO_2 and MnO_2-pGO nanocomposite agreed well with the regular compound K-birnessite MnO_2 (JCPDS card 80-1098) with the diffraction peaks appeared at 2θ =11.7° (001), 21.8° (002), 36.7° (100), 41.8° (102) 55.5 (103), and 66. 1° (110) respectively, indicating that MnO_2 was generated. [34] In addition the interlayer spacing of (001), (002), (100), (102), (103), and (110) reflection planes were nearly 0.75, 0.40, 0.24, 0.2, 0.16 and 0.14 nm attributed to the presence of k^+ and H_2O molecules in the interlamination.[35] In addition, the intensity of (002), (102), and (103) plane reflection peaks in the MnO_2-pGO composite weakened after hybridizing with pGO. This could be ascribed to the MnO_2 crystals deposited on pGO sheets which inhibit themselves from growing to be complete crystals, result much lower crystallinity.[36]

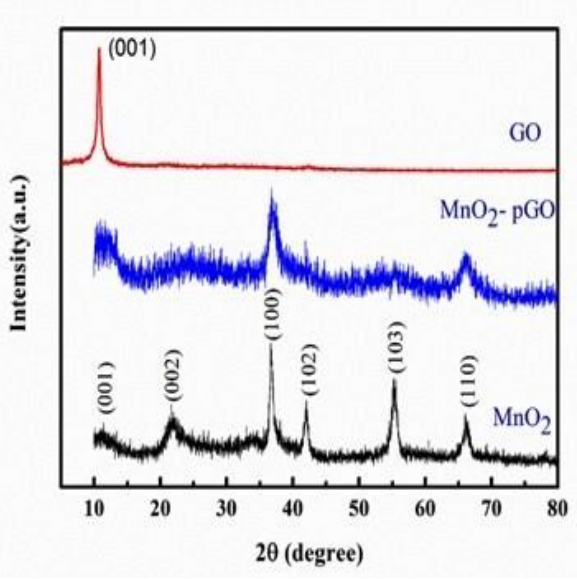

Fig. 1: XRD pattern of GO, MnO_2-pGO composite and the pure MnO_2.

The FT-IR spectra of the samples are shown in Fig 3. The spectrum of GO illustrating the ─OH stretching vibration at 3428 cm^{-1}, the C═O stretching mode at 1701 cm^{-1}, the aromatic C═C stretching at 1627 cm^{-1}, the C─O (carboxyl) stretching mode at 1365 cm^{-1}, the C─O (epoxyl) stretching mode at 1230 cm^{-1} and the C─O (alkoxyl) stretching vibration at 1085 cm^{-1}.[33] After hybridization, the characteristic peaks of ─OH (3428), C═C (1627), C─OH (1469), C─O (epoxyl, 1365), C─O (alkoxyl, 1085) and Mn─O (515 cm^{-1}) were detected in the spectrum of the composite, suggesting the successful synthesis of the MnO_2-pGO. In addition, the peak intensity of these functional groups are reduced, or even diminish (at around 3428 and 1230 cm^{-1} for C═O and C─O (epoxyl), demonstrating partial reduction of GO into pGO.[37] The existence Mn─O bond suggests that MnO_2 were produced and grafted on the surface of pGO, during the reaction process.[38] Moreover, the simultaneous manifestation of bands in the region 2920 and 2851 cm^{-1} nearby in the MnO_2-pGO belong to methyl groups (C-H), which might be due to residual surfactant even after washing with water and ethanol. In the XPS survey-scan spectrum of MnO_2-pGO nanocomposite (Fig. 4a), the typical C 1s, O 1s, and Mn 2p peaks were observed, suggesting the presence of GO and MnO_2 in composite. Notably, K is also detected on the survey spectrum since K^+ is a balance charge of negatively-charged MnO_2 layers. In Fig. 4b and Fig. S1, the C 1s spectra of the MnO_2-pGO and GO, is deconvoluted into several symmetrical peaks. Four peaks centered at 284.0 (C═C), 285.9 (C─OH/ C─ O ─C), 287.5 (C═O), and 288.4 eV (HO─ C ═O) were observed in both of Fig. 4. b and Fig. S1 [39]. In case of MnO_2-pGO, the peak intensity of aromatic C═C (284.4 eV) is dramatically increased while that of (C─OH/ C─ O ─C), (C═O), and (HO─ C ═O) are partially decreased or even reduced (C═O), as the reaction time prolonged, which is consistent well with the results of FT-IR analysis. In the XPS spectra of O 1s (Fig 4c) the peak located at 531.0 eV is assigned to the oxygen bonded with manganese (O-Mn) [40] and the peak appeared at 529.0 eV is attributed to oxygen bonded with carbon (O-C).[41] In Fig 4(d) appearance of two peaks centered at 653.7 and 642.0 eV can be ascribed to Mn ($2p_{1/2}$) and Mn ($2p_{3/2}$), signifying the existence of Mn^{2+} oxidation state in the composite respectively. They have a spin-energy separation of 11.7 eV, which correlates with earlier reported data of Mn ($2p_{1/2}$) and Mn ($2p_{3/2}$) in MnO_2 [42]. In addition, according to the survey scan of XPS analysis, the mass of C, Mn, O and K was about 36.52%, 18.6%, 42.98%, and 1.9%, respectively.

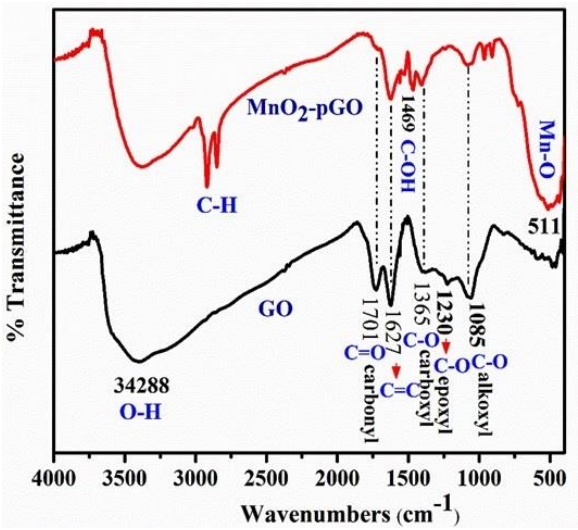

Fig. 2: FT-IR spectra of GO and MnO_2-pGO nanocomposite.

The corresponding energy-dispersive X-ray spectrometry (EDX) mapping and spectrum analysis of MnO_2-pGO composite Fig. 1(B) unambiguously confirms the uniform distribution and the manifestation of Mn, O and C elements, and the homogeneous distribution of MnO_2 over the GO surface in the MnO_2-pGO composite[43]. The atomic percentages (see Table.S1) of C, O and Mn are 43.170, 34.293 and 22.536, respectively.

The typical Raman spectra of the GO, pure MnO_2 and MnO_2-pGO nanocomposite are shown in Fig. 5. In Fig. 5(a) the two diagnostic peaks of GO, the D and G band are observed around 1345 cm^{-1} and 1597 cm^{-1}, assign to the breathing mode of aromatic six member sp^2 carbon rings and the bond stretching mode of sp^2 carbon atoms[44].The Sharp peak at 644 cm^{-1} is ascribed to the Mn─O lattice vibration perpendicular to the direction of MnO_6 octahedral double chain of MnO_2 [45], which is in well agreement with pure MnO_2 shown in Fig. 5(b). The analysis further endorses the yield of MnO_2 and graphene oxide composite have been accomplished

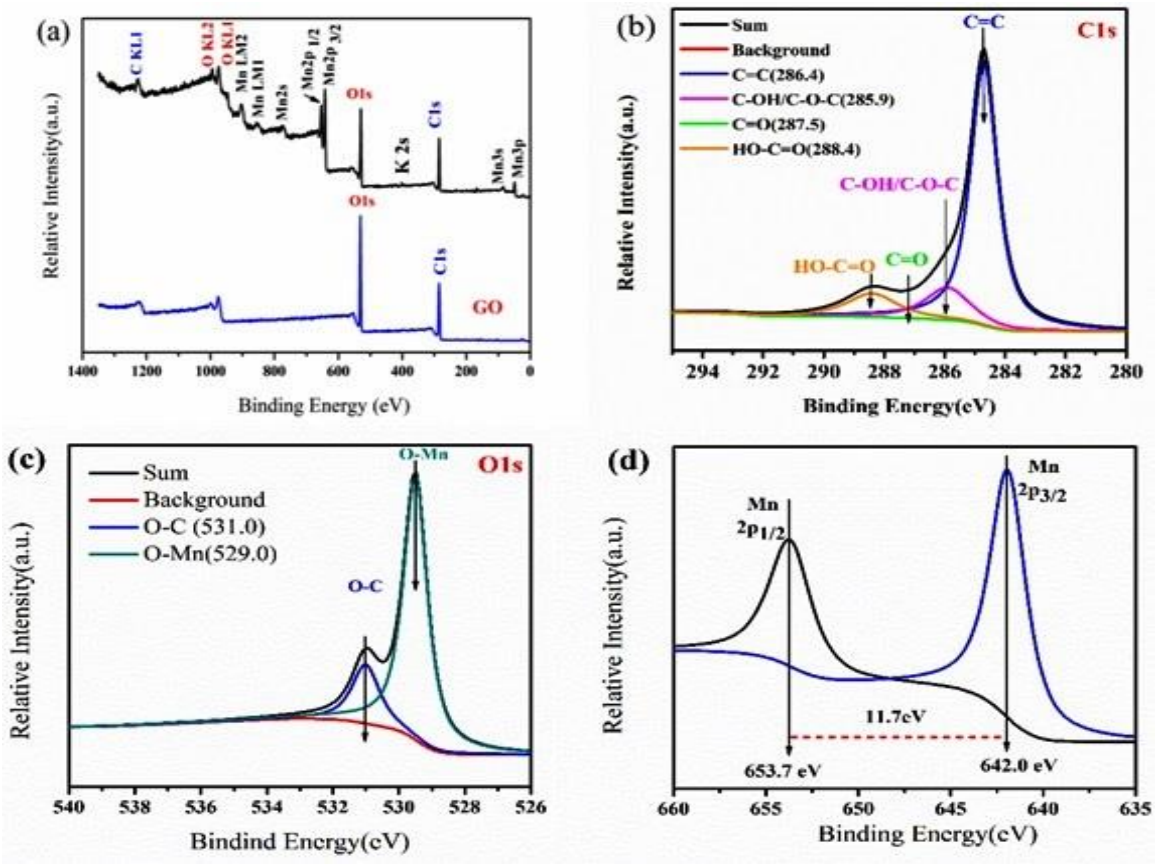

Fig. 3: XPS spectra of the MnO_2-pGO nanocomposite: (a) survey-scan spectrum; (b) high-resolution C 1s spectrum; (c) high-resolution O 1s spectra and (d) high-resolution Mn 2p spectra respectively.

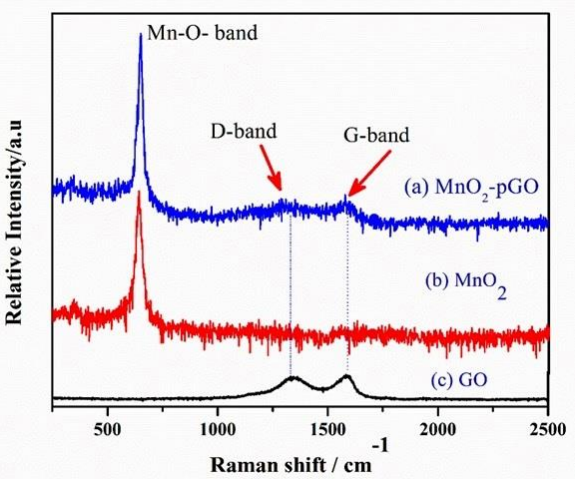

Fig. 4: (a) Raman spectra for MnO_2-pGO nanocomposite; (b) for MnO_2 and (c) for GO.

The SEM images of pure of pure MnO_2 and MnO_2-pGO nanocomposite are shown in Fig. 6. The low and high resolutions images of pure MnO_2, (Fig. 6 a, b), depicts hierarchical porous MnO_2 nanocluster, which were self-assembled desultorily from elongated nanorods with an average size of nearly ~57-190 nm. The SEM image of MnO_2-pGO composite in Fig. 6(c and d) showed that the elongated nanostructures of MnO_2 (Fig. S2 the other images) are grafted and homogeneously covered all the surface of pGO sheets. The reflection well agreement with the homogeneous distribution of the Mn, O and C elements, concluded from the corresponding EDS mapping analysis Fig. 1 (B). Furthermore, the pGO sheets exhibit porous folded crumples structure (Fig. 6c), which are favorable for providing fast electrolyte diffusion channels with a low activation barrier than that of a smooth graphene sheets [46]. Moreover, the TEM image in Fig. 7 (a low and the inset high magnification) shows pure MnO_2 exhibits rode-like morphology with an average diameter of ~3-12 nm and an average length of ~ 19.7 to 49.9 nm. The TEM image of MnO_2-pGO nanocomposite in Fig. 7 (b and c) revealed the layered structure of pGO sheets appeared in a transparent swollen state, uniformly coated with MnO_2 nanorods, corresponding well to the results of SEM analysis. The image also suggest robust collaboration between pGO sheets and MnO_2 layers through electrostatic attraction, physisorption or charge-transfer interactions.[47] As can be seen in Fig. 7 (d), HR-TEM image displays the well-defined lattice fringes with interplaner distance of 0.24 nm and 0.14nm. This result is agreement well with the interplanar spacing between the (100) and (110) crystal planes of K-birnessite MnO_2 [48] and similarly consistent with XRD results.

For further characterization of the porous structure of the prepared pure MnO_2 and MnO_2-pGO composite the N_2 adsorption-desorption isotherm and the pore size distribution curves were probed by measuring nitrogen adsorption-desorption isotherms. As shown in Fig. 8, both the samples (pure MnO_2 and MnO_2-pGO composites) were found to exhibit similar, type IV adsorption/desorption isotherm, with an H1-type hysteresis loop, suggesting mesoporous nature of the samples.[49] The textural properties and parameters, such as BET specific surface area (SA_{BET}), the total pore volumes (V_T) and pore size (PS_{BJH}) of the composite are calculated and are précised in Table-1. The BET specific surface area of MnO_2-pGO is (121.0 m^2 g^{-1}), which is greater than pure MnO_2 (101.6 m^2 g^{-1}). Moreover, the pore size distribution calculated from PS_{BJH} shows that the pores created by both the pure MnO_2 and MnO_2-pGO nanocomposite (as shown inset image of Fig. 9), are mesoporous structure with an average pore size of ~5.1 and ~6.0 nm. The corresponding pore volume is 1.301 and 1.301 m^3g^{-1} for pure MnO_2 and the MnO_2-pGO nanocomposite, respectively. It is reasonable to believe that the introduction of pGO in the composite enhanced the aggregation of MnO_2 particles on its surface(pGO), thus leading to a high surface area which are beneficial to the kinetics of electrochemical process.[50].

Table-1: Summary of nitrogen sorption porosimetry studies parameters of as-synthesized pure MnO_2 and MnO_2-pGO nanocomposites.

Sample	$S.A_{BET}$ (m^2 g^{-1})	Pore volume (cm^3 g^{-1})	Mean pore size (nm)
Pure MnO_2	**101.60**	**1.301**	**5.120**
MnO_2-pGO	**121.60**	**1.625**	**6.066**

Surface areas (S.A) determined by the BET analysis, mean pore diameters by BHJ theory and pore volumes by single-point study

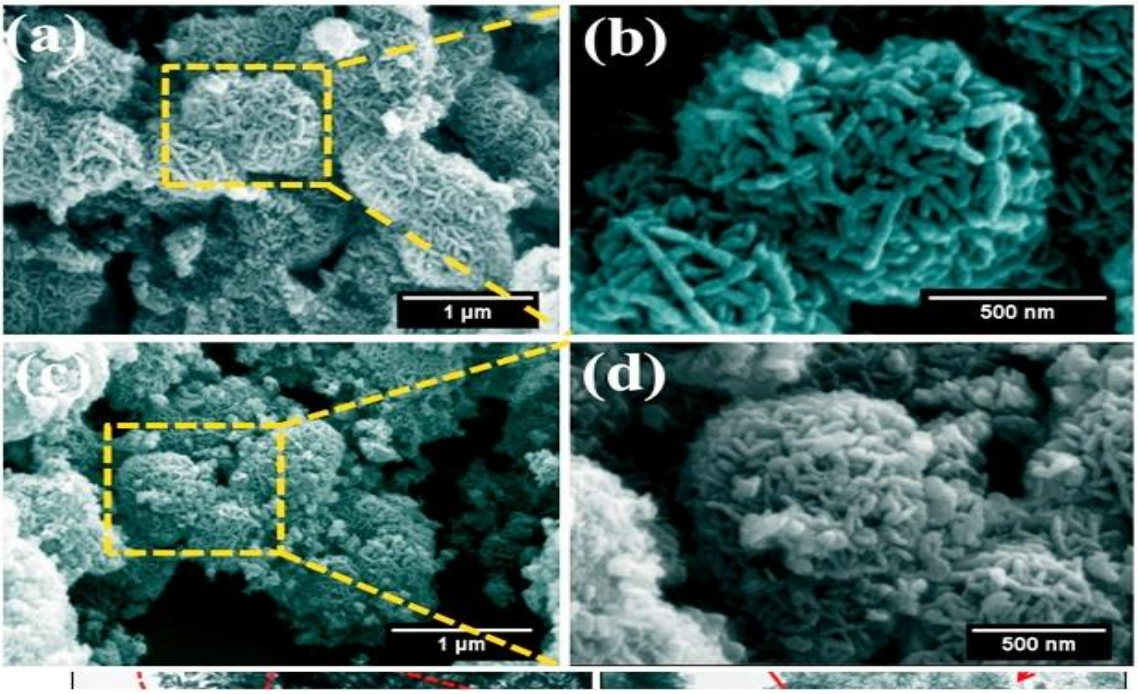

Fig. 5: (a-b) SEM image for pure MnO_2 and (c-d) SEM image for MnO2-pGO nanocomposite (low and high resolution) respectively.

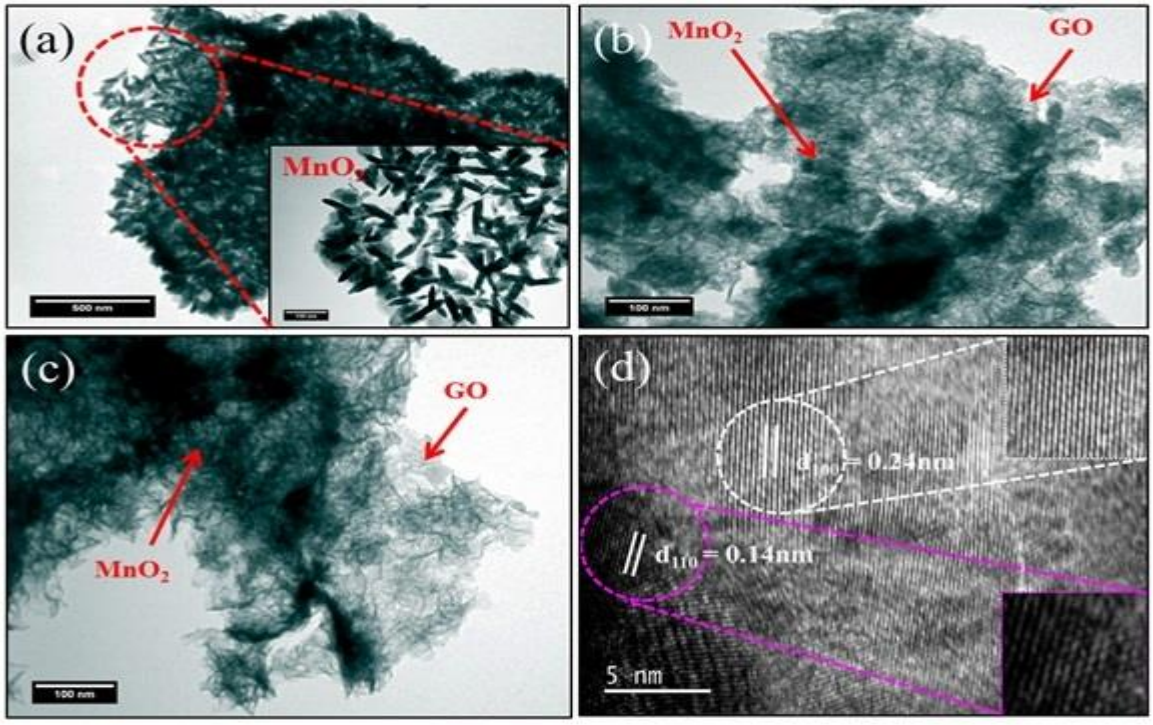

Fig. 6: (a) TEM image for pure MnO_2 (b-c) TEM image for MnO_2-pGO nanocomposite and (d) HR-TEM micrograph for MnO_2-pGO nanocomposite.

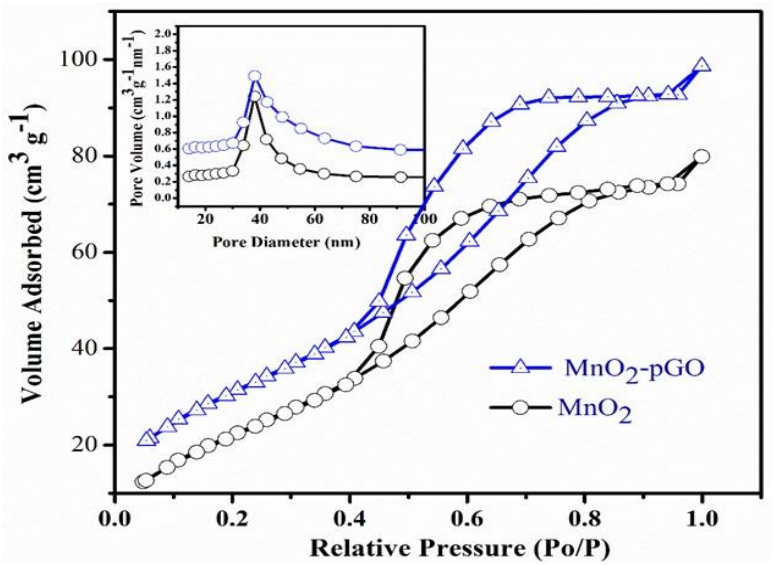

Fig. 7: The Nitrogen adsorption-desorption isotherms and the corresponding pore size distribution plots (inset image) of pure MnO_2 and MnO_2-pGO nanocomposites respectively.

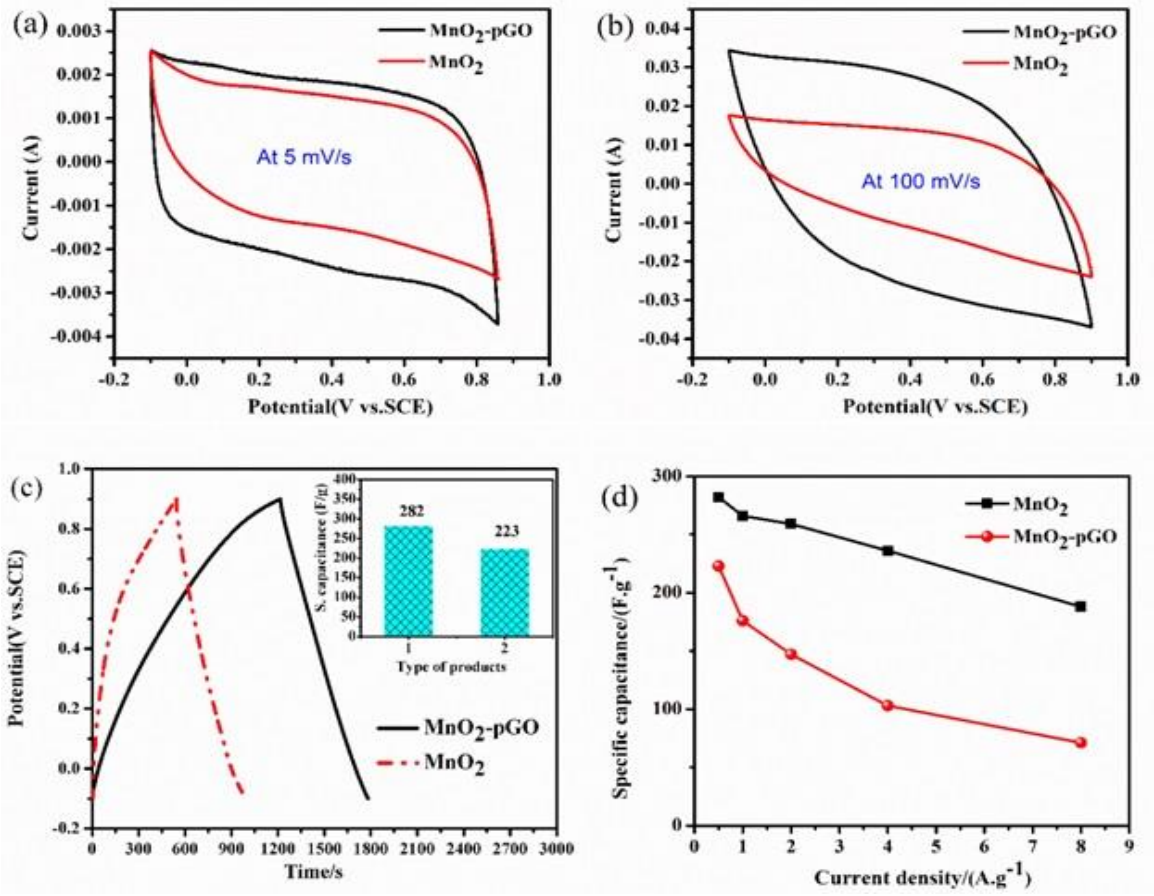

Fig. 8: (a) CV curves of pure MnO_2 and MnO_2-pGO nanocomposite at 5 mVs^{-1}; (b) CV curves at 100 mVs^{-1}; (c) GCD curves at a constant current density of 0.5 Ag^{-1}, inset shows the histogram of the specific capacitance of the samples at 0.5 Ag^{-1} and (d) specific capacitance at various current densities.

Electrochemical studies

Fig 9 (a) shows typical cyclic voltammograms (CV) of pure MnO_2 and the MnO_2-pGO nanocomposite at the sweep rate of 5 mV/s. Rectangular shape and mirror image of CV loop is a fingerprint for the capacitance behavior of any material.[51] It can be seen that, both the curves exhibits an obvious rectangular nature of the CV plot, which confirms the redox reactions are proceeding during the charge/discharge processes. Based on the perception anticipated by chan.et.al., [52] alkali metal cations (Na^+) could rapidly intercalated / de-intercalated into the bulk of MnO_2, as soon as the electrode was dipped into the electrolyte (1 M Na_2SO_4), so the reversible redox reactions could be represented as;

$$MnO_2 + H^+ + e^- \leftrightharpoons MnOOH \quad (2)$$

$$MnO_2 + Na^+ + e- \leftrightharpoons MnOONa \quad (3)$$

$$(MnO_2)\ surface + Na^+ \leftrightharpoons MnOONa^+ \quad (4)$$

Moreover, the integral areas of the CV curve for MnO_2-pGO nanocomposite is greater than that of pure MnO_2 electrode (MnO_2-pGO > pure MnO_2), suggesting higher specific capacitance (SC) and fast charge circulation within the electrode surface. Fig. 9 (b) shows the comparative CV curves of pure MnO_2 and MnO_2-pGO nanocomposite at a very high scan rate of 100 mV/s. It is observed that, the CV curve of pure MnO_2 electrode shows quit deviation from the rectangular shape at a high scan rate of 100 mV/s. However, MnO_2-pGO nanocomposite electrode display CV curve of nearly rectangular shape, with no severe distortion of the symmetry, showing a comparatively good capacitive behavior under the high scan rate of 100 mV/s, which were mainly ascribed to the synergistic effect between conductive pGO and MnO_2 as reported earlier.[43]

The galvanostatic charge-discharge (GCD) curves of pure MnO_2 and the MnO_2-pGO nanocomposite at $0.5Ag^{-1}$ are demonstrated in Fig. 9(c). The GCD curves of both the electrode shows linear and triangular symmetry, indicating an ideal capacitive behavior during the redox process.[32] The discharge time for MnO_2-pGO nanocomposite electrode comparatively longest, suggesting good energy storage performance. At a current density of 0.5 A/g, the SC was estimated to be 223 F/g for pure MnO_2 and 282 F/g for MnO_2-pGO (as shown inset of Fig. 9c). Fig. 9 (d) illustrate the SC of pure MnO_2 and MnO_2-pGO at various current densities of 0.5, 1, 2, 4, and 8 A/g. MnO_2-pGO revealed obviously higher specific capacitances than that of the pure MnO_2 at any current density. The SC of MnO_2-pGO was calculated to be 282, 266, 259, 236, and 188 F/g with retention rates of 66.7 %. Similarly, the SC of pure MnO_2 was 223, 176, 147, 103, and 71 F/g, with retention rates of 32.0 %. Consequently, the rate capability of MnO_2-pGO nanocomposite electrode was remarkably enhanced compared with pure MnO_2 electrode. It can be attributed to the excellent electron conductivity and electrode stability of pGO, in the nanocomposite.

On the basis of the above information, MnO2-pGO electrode was selected for further detail electrochemical analysis. Fig. 10 (a) shows the rate-dependent CV curves for MnO_2-pGO nanocomposite electrode with the scan rates range of 5−50 mV/s. It can be seen that, at a low scan rate of 5,10 and 20 mV/s the CV curves show standard rectangular shape, signifying ideal pseudocapacitive performance and low charge contact resistance.[41] Furthermore, with increasing scan rate (50-100 mV/s), the total current increases in the CV curves, clearly indicating the shape does not change significantly, suggesting a good rate capability and diffusion-controlled phenomenon. [53] Fig. 10 (b) illustrates the GCD curve of MnO_2-PGO nanocomposite electrode at different current densities range of 0.5−8 A/g. It can be observed that, all the charge curves are highly linear to their corresponding discharge counterpart, signifying the Faradaic reactions along with double layer contribution.[47] Furthermore, the long discharging time of the curve at 0.5 A/g, demonstrated higher SC, hence verifying the CV results. In addition, the SC decreasing as the increasing current densities, which could be attributed to the high resistance and lower Faradaic redox reactions under higher current densities.[21] The enhanced electrochemical performance of MnO_2-pGO predominantly attributed to its unique nanoarchitectures (hierarchical elongated nanorod) of MnO_2 obtained in vesicle solution route are around 3-12 nm in diameter, which provides an efficient surface area for effective pseudocapacitive reaction between MnO_2 and electrolyte. . The excellent support of pGO carbon matrix allowed the strong deposition of MnO_2 nanoparticles, which enhanced the mechanical strength of nanocomposite materials and MnO_2 could act as a spacer to avoid restacking of pGO sheets, thus forming a 3D network structure with large electrochemically active surface area leads to better conductivity and effective diffusion of electrolyte in the nanocomposite.

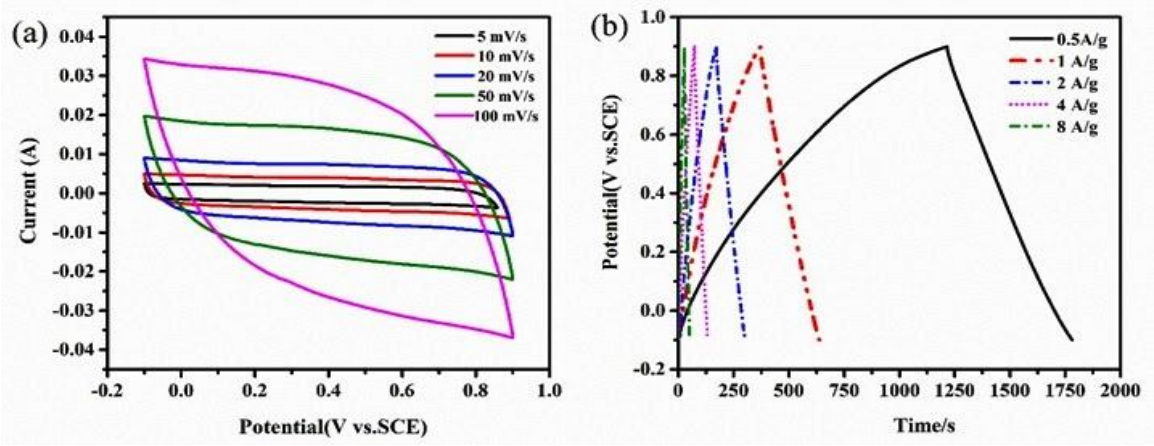

Fig. 9: (a) CV curve of MnO_2-pGO composite electrode at various scan rate and (b) GCD curves at various current density.

The resistive characteristics of the samples electrodes (MnO_2 and MnO_2-pGO), was analyzed by electrochemical impedance analysis (EIS), are illustrated in Fig. 11. The Nyquist plots of both the sample electrodes exhibit an imperfect small arc in the high-frequency region and a nonstraight line in the low-frequency regime. In general, for a typical electrode-electrolyte system, the semicircle diameter in the high-frequency regime represents charge-transfer resistance (R_{CT}) at the electrode/electrolyte interface [54], while the slope of the line intercept to the real axis (between 45º to 90º) related to capacitive nature and ions diffusion resistance in the samples.[55] As can be seen the enlarge image in the inset part of Fig. 11, the diameter increased in order of MnO_2-pGO < MnO_2 and the R_{CT} were calculated to be 2.032 Ω for MnO_2-pGO and 2.147 Ω for MnO_2. The slope of MnO_2-pGO slightly greater than pure MnO_2, indicating that MnO_2-pGO embrace the lowest R_{CT}, the good capacitive performance, and the lowest ions diffusion resistance, [56] compared to pure MnO_2. The results further suggest that MnO2-pGO possessed the enhanced electrochemical performance suitable to be used electrode energy material of supercapacitor applications.

Meanwhile a long term cycling stability and Coulombic efficiency test was investigated upto 1200 cycles for pure MnO_2 and 5000 cycles for MnO_2-pGO nanocomposite at current density of 4 A/g and the results are demonstrated in Fig. S3 and Fig. 12. After 1200 and 5000 cycles, pure MnO_2 and MnO_2-pGO nanocomposite remained 64.0% and 91.4% of their initial specific capacitance with ~100% Coulombic efficiency, respectively. MnO_2-pGO nanocomposite reveals clearly the excellent long term retention capability, demonstrating high electron and electrolyte transportation in the nanocomposite.[57] Furthermore, Nyquist was implemented to explore the motive for the enhanced specific capacitance and stable capacitance retention of MnO_2-pGO nanocomposite before and after a 5000 cycles test. The Nyquist plots of MnO_2-pGO before and after cycles test are shown in Fig. S4. As can be seen in the high frequency region, (the inset part of Fig. S4), there is not substantial changes arise in the diameter of the curves before and after 5000 cycles test, although there is slight decrease can be observed in the slope line intercept to the real axis. The R_{CT} were calculated to be 2.032 Ω before and 2.733 Ω after 5000 cycles for MnO_2-pGO

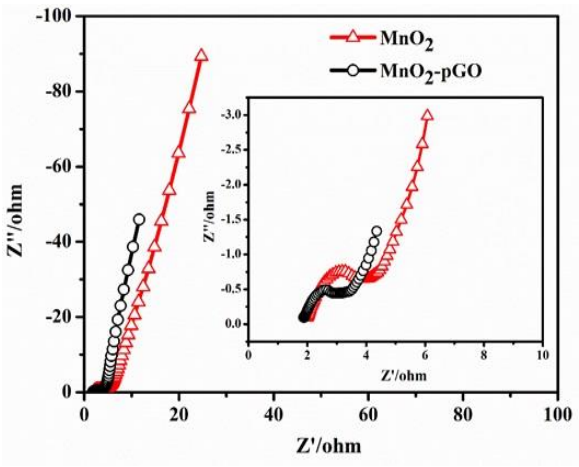

Fig. 10: Nyquist plots of the EIS data for the pure MnO_2 and MnO_2-pGO nanocomposite electrode.

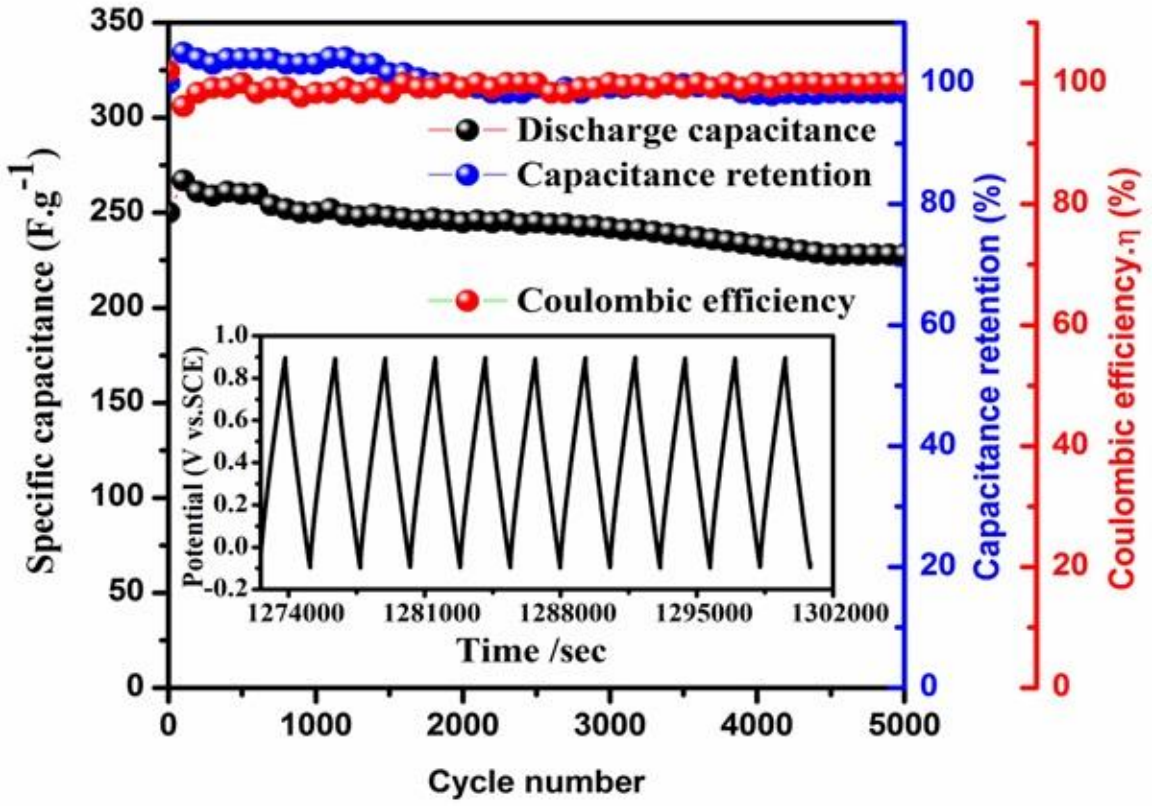

Fig. 11: Specific capacitance and Coulombic efficiency (η) of MnO_2-pGO nanocomposite electrode as a function of cycle number at the current density of 4 Ag^{-1} (inset shows corresponding last few charge/discharge cycles).

Conclusion

In conclusion, nanocomposite of MnO_2-pGO was successfully synthesized using vesicle solution approach, via surfactant hexadecyltrimethyl ammonium bromide (CTAB) and sodium dodecyl benzene sulfonate (SDBS), as a structure-directing agent. Our analysis revealed that manganese oxide (MnO_2) nanocluster, which were self-assembled from elongated nanorods were generated on pGO sheet during the prolonged reaction time. More importantly, the fabricated MnO_2-pGO nanocomposite endow excellent ECPs, like high SC (282 F g^{-1}), the good rate capability (67.7%) at 10 A/g), the stable capacitance retention (91.4 %after 5000 cycles), and the ~100% Coulombic efficiency, making it to become a promising electrode energy material to be used in supercapacitor application.

Acknowledgment

We thankfully acknowledge the support of this work by the National Natural Science Foundation of China (No.21501104) the Natural Science foundation of Heilongjiang Province (B2015014)

References

1. C. Zhang, Y.-L. Wei, P.-F. Cao, and M.-C. Lin, "Energy storage system: Current studies on batteries and power condition system," *Renew. Sustain. Energy Rev* **82**, 3091 (2018).
2. R. S. Kate, S. A. Khalate, and R. J. Deokate, "Overview of nanostructured metal oxides and pure nickel oxide (NiO) electrodes for supercapacitors: A review," *J. Alloys Compd.*, **734**, 89 (2018).
3. E. Goikolea and R. Mysyk, "Chapter Four - Nanotechnology in Electrochemical Capacitors," Micro and Nano Tecnol., 7, 131 (2017).
4. F. Chen, L. Wang, X. Ji, and Q. Zhang, "Temperature-Dependent Two-Dimensional Transition Metal Dichalcogenide Heterostructures: Controlled Synthesis and Their Properties," *ACS Appl. Mater. Interfaces.*, **9**, 30821 (2017).
5. J. Zhou, B. Tang, J. Lin, D. Lv, J. Shi, L. Sun, Q.

Zeng, L. Niu, F. Liu, *et al*., "Morphology Engineering in Monolayer MoS2-WS2 Lateral Heterostructures," *Adv. Funct. Mater.,* **28**, 1801568 (2018).

6. C. Huang and Q. Cheng, "Learning from nacre: Constructing polymer nanocomposites," *Compos. Sci. Technol.,* **150**, 141 (2017).
7. M. Ishaq, M. Jabeen, W. Song, L. Xu, and Q. Deng, "3D hierarchical Ni2+/Mn2+/Al3+ layered triple hydroxide @ nitrogen-doped graphene wrapped hybrids on nickel foam for supercapacitor applications," *J. Electroanal. Chem.,* **804**, 220 (2017).
8. M. Jabeen, M. Ishaq, W. Song, L. Xu, and Q. Deng, "Synthesis of Ni/Co/Al-layered triple hydroxide@brominated graphene hybrid on nickel foam as electrode material for high-performance supercapacitors," *RSC Adv.* **7**, 46553 (2017).
9. M. Jabeen, M. Ishaq, W. Song, L. Xu, I. Maqsood, and Q. Deng, "UV-Assisted Photocatalytic Synthesis of ZnO-Reduced Graphene Oxide Nanocomposites with Enhanced Photocatalytic Performance in Degradation of Methylene Blue," *ECS J. Solid State Sci. Technol.,* **6** , M36 (2017).
10. B. Kirubasankar, P. Palanisamy, S. Arunachalam, V. Murugadoss, and S. Angaiah, "2D MoSe2-Ni(OH)2 nanohybrid as an efficient electrode material with high rate capability for asymmetric supercapacitor applications," *Chem. Eng. J.,* **355**, 881 (2019).
11. D. Li, R. Li, M. Lu, X. Lin, Y. Zhan, and L. Jiang, "Carbon dioxide reforming of methane over Ru catalysts supported on Mg-Al oxides: A highly dispersed and stable Ru/Mg(Al)O catalyst," *Appl. Catal. B Environ.,***200**, 566 (2017).
12. X. Ou, Q. Li, D. Xu, J. Guo, and F. Yan, "In Situ Growth of MnO2 Nanosheets on N-Doped Carbon Nanotubes Derived from Polypyrrole Tubes for Supercapacitors," *Chem. – An Asian J.* **13**, 545 (2018).
13. L. W. Ye, Y. F. Yuan, L. N. Wang, M. Zhu, S. M. Yin, Y. B. Chen, and S. Y. Guo, "NiCo2S4/Co3S4 heterogeneous double-shelled nanocages for high-performance electrochemical energy storage," *Mater. Lett.,* **229**, 152 (2018).
14. K. Khawas, P. Kumari, S. Daripa, R. Oraon, and B. K. Kuila, "Hierarchical Polyaniline-MnO2-Reduced Graphene Oxide Ternary Nanostructures with Whiskers-Like Polyaniline for Supercapacitor Application," *Chem.Select* **2**, 11783 (2017).
15. Y. Zhao, M. P. Li, S. Liu, and M. F. Islam, "Superelastic Pseudocapacitors from Freestanding MnO2-Decorated Graphene-Coated Carbon Nanotube Aerogels," *ACS Appl. Mater. Interfaces.,* **9**, 23810 (2017).
16. P. Wang, Y.-J. Zhao, L.-X. Wen, J.-F. Chen, and Z.-G. Lei, "Ultrasound–Microwave-Assisted Synthesis of MnO2 Supercapacitor Electrode Materials," *Ind. Eng. Chem. Res.,* **53**, 20116 (2014).
17. H. Shen, Y. Zhang, X. Song, Y. Liu, H. Wang, H. Duan, and X. Kong, "Facile hydrothermal synthesis of actiniaria-shaped α-MnO2/activated carbon and its electrochemical performances of supercapacitor," *J. Alloys Compd.,***770**, 926 (2019).
18. Z. Pan, M. Liu, J. Yang, Y. Qiu, W. Li, Y. Xu, X. Zhang, and Y. Zhang, "High Electroactive Material Loading on a Carbon Nanotube@3D Graphene Aerogel for High-Performance Flexible All-Solid-State Asymmetric Supercapacitors," *Adv. Funct. Mater.,* **27**, 1701122 (2017).
19. C.-M. Yang and B.-H. Kim, "Highly conductive pitch-based carbon nanofiber/MnO2 composites for high-capacitance supercapacitors," *J. Alloys Compd.,* **749**, 441 (2018).
20. B. Amutha, K. Subramani, P. N. Reddy, and M. Sathish, "Graphene-Polymer//Graphene-Manganese Oxide Nanocomposites-Based Asymmetric High Energy Supercapacitor with 1.8 V Cell Voltage in Aqueous Solution," *Chem.Select.,* **2**, 10754 (2017).
21. F. Z. Amir, V. H. Pham, E. M. Schultheis, and J. H. Dickerson, "Flexible, all-solid-state, high-cell potential supercapacitors based on holey reduced graphene oxide/manganese dioxide nanosheets," *Electrochim. Acta.,* **260**, 944 (2018).
22. 22. P. C. Ooi, M. A. S. M. Haniff, M. F. M. R. Wee, C. F. Dee, B. T. Goh, M. A. Mohamed, and B. Y. Majlis, "Reduced graphene oxide preparation and its applications in solution-processed write-once-read-many-times graphene-based memory device," *Carbon N. Y.,* **124**, 547 (2017).
23. K. S. Lee, C. W. Park, S. J. Lee, and J.-D. Kim, "Hierarchical zinc oxide/graphene oxide composites for energy storage devices," *J. Alloys Compd.,* **739**, 522 (2018).
24. M. R. Karim, K. Hatakeyama, T. Matsui, H. Takehira, T. Taniguchi, M. Koinuma, Y. Matsumoto, T. Akutagawa, T. Nakamura, *et al*., "Graphene Oxide Nanosheet with High Proton Conductivity," *J. Am. Chem. Soc.,* **135**, 8097 (2013).
25. Z. Gao, W. Yang, J. Wang, B. Wang, Z. Li, Q. Liu, M. Zhang, and L. Liu, "A New Partially Reduced Graphene Oxide Nanosheet/Polyaniline

Nanowafer Hybrid as Supercapacitor Electrode Material," *Energy & Fuels.*, **27**, 568 (2013).
26. W. Yan, W.-J. Yu, L. Wang, D. Zhang, X.-Q. Ge, J.-Z. Hang, W. Deng, and L.-Y. Shi, "Preparation of Partially Reduced Graphene Oxide Nanosheets/Poly(Sodium 4-Styrenesulfonate) Composite with High Capacitance," *Electrochim. Acta.*, **147**, 257 (2014).
27. R. Dong, W. Liu, and J. Hao, "Soft Vesicles in the Synthesis of Hard Materials," *Acc. Chem. Res.*, **45**, 504 (2012).
28. X. Luo, Z. Pan, F. Pei, Z. Jin, K. Miao, P. Yang, H. Qian, Q. Chen, and G. Feng, "In situ growth of hollow Cu2O spheres using anionic vesicles as soft templates," *J. Ind. Eng. Chem.*, **59**, 410 (2018).
29. N. I. Zaaba, K. L. Foo, U. Hashim, S. J. Tan, W.-W. Liu, and C. H. Voon, "Synthesis of Graphene Oxide using Modified Hummers Method: Solvent Influence," *Procedia Eng.*, **184**, 469 (2017).
30. M. Jabeen, M. Ishaq, W. Song, L. Xu, I. Maqsood, and Q. Deng, "UV-Assisted Photocatalytic Synthesis of ZnO-Reduced Graphene Oxide Nanocomposites with Enhanced Photocatalytic Performance in Degradation of Methylene Blue," *ECS J. Solid State Sci. Technol.*, **6**, M36 (2017).
31. M. Ishaq, M. Jabeen, W. Song, L. Xu, W. Li, and Q. Deng, "Fluorinated graphene-supported Nickel-Cobalt-Iron nitride nanoparticles as a promising hybrid electrode for supercapacitor applications," *Electrochim. Acta*., **282**, 913 (2018).
32. X. Bai, X. Tong, Y. Gao, W. Zhu, C. Fu, J. Ma, T. Tan, C. Wang, Y. Luo, *et al*., "Hierarchical multidimensional MnO2 via hydrothermal synthesis for high performance supercapacitors," *Electrochim. Acta.*, **281**, 525 (2018).
33. B. Paulchamy, G. Arthi, and L. Bd, "A Simple Approach to Stepwise Synthesis of Graphene Oxide,"*J Nanomed Nanotechnol*.,6, 253 (2015).
34. P. Iamprasertkun, A. Krittayavathananon, A. Seubsai, N. Chanlek, P. Kidkhunthod, W. Sangthong, S. Maensiri, R. Yimnirun, S. Nilmoung, *et al*., "Charge storage mechanisms of manganese oxide nanosheets and N-doped reduced graphene oxide aerogel for high-performance asymmetric supercapacitors," *sci. Report.*, 6, 37560 (2016).
35. F. Ochai-Ejeh, M. J. Madito, K. Makgopa, M. N. Rantho, O. Olaniyan, and N. Manyala, "Electrochemical performance of hybrid supercapacitor device based on birnessite-type manganese oxide decorated on uncapped carbon nanotubes and porous activated carbon nanostructures," *Electrochim. Acta.*, **289**, 363 (2018).
36. G. Wang, Z. Wei, and Q. Min, "morphology , crystallization and mechanical properties of poly(e-caprolactone)/graphene oxide nanocomposites," *Chinese j. Poly.Sci.*, 31 1148 (2013).
37. N. R. Nirala, S. Abraham, V. Kumar, S. A. Pandey, U. Yadav, M. Srivastava, S. K. Srivastava, V. N. Singh, A. M. Kayastha, *et al*., "Partially reduced graphene oxide–gold nanorods composite based bioelectrode of improved sensing performance," *Talanta.*, **144**, 745 (2015).
38. Z. Song, Y.-L. Ma, and C.-E. Li, "The residual tetracycline in pharmaceutical wastewater was effectively removed by using MnO2/graphene nanocomposite," *Sci. Total Environ.*, **651**, 580 (2019).
39. X. Xu, L. Pan, Y. Liu, T. Lu, Z. Sun, and D. H. C. Chua, "Facile synthesis of novel graphene sponge for high performance capacitive deionization.," *Sci. Rep.*, **5**, 8458 (2015).
40. H. Lv, Y. Yuan, Q. Xu, H. Liu, Y.-G. Wang, and Y. Xia, "Carbon quantum dots anchoring MnO2/graphene aerogel exhibits excellent performance as electrode materials for supercapacitor," *J. Power Sources.*, **398**, 167 (2018).
41. W. Xiao, W. Zhou, H. Yu, Y. Pu, Y. Zhang, and C. Hu, "Template synthesis of hierarchical mesoporous δ-MnO2 hollow microspheres as electrode material for high-performance symmetric supercapacitor," *Electrochim. Acta.*, **264**, 1 (2018).
42. B. Wei, L. Wang, Q. Miao, Y. Yuan, P. Dong, R. Vajtai, and W. Fei, "Fabrication of manganese oxide / three-dimensional reduced graphene oxide composites as the supercapacitors by a reverse microemulsion method," *Carbon N. Y.*, **85**, 249 (2015).
43. M. Ramezani, M. Fathi, and F. Mahboubi, "Facile synthesis of ternary MnO2/graphene nanosheets/carbon nanotubes composites with high rate capability for supercapacitor applications," *Electrochim. Acta.*, **174**, 345 (2015).
44. P. Cao, L. Wang, Y. Xu, Y. Fu, and X. Ma, "Facile hydrothermal synthesis of mesoporous nickel oxide/reduced graphene oxide composites for high performance electrochemical supercapacitor," *Electrochim. Acta.*, **157**, 359 (2015).
45. T. Jia-yong, "Synthesis of a Mesoporous Manganese Dioxide-Graphene Composite by a

Simple Template-Free Strategy for High-Performance," *Acta Phys. - Chim. Sin.*, **30**, 1876 (2014).

46. S. Deng and V. Berry, "Wrinkled, rippled and crumpled graphene: An overview of formation mechanism, electronic properties, and applications," *Mater. Today.*, **19**, 197 (2016).
47. Y. Chen, J. Zhang, M. Li, C. Yang, L. Zhang, C. Wang, and H. Lu, "Strong interface coupling and few-crystalline MnO2/Reduced graphene oxide composites for supercapacitors with high cycle stability," *Electrochim. Acta., 9, 131*(2018).
48. X. Zhang, M. He, P. He, C. Li, H. Liu, X. Zhang, and Y. Ma, "Ultrafine nano-network structured bacterial cellulose as reductant and bridging ligands to fabricate ultrathin K-birnessite type MnO2 nanosheets for supercapacitors," *Appl. Surf. Sci.*, **433**, 419 (2018).
49. S. R. Srither, A. Karthik, S. Arunmetha, D. Murugesan, and V. Rajendran, "Electrochemical supercapacitor studies of porous MnO2 nanoparticles in neutral electrolytes," *Mater. Chem. Phys.*, **183**, 375 (2016).
50. Z.-S. Wu, W. Ren, D.-W. Wang, F. Li, B. Liu, and H.-M. Cheng, "High-Energy MnO2 Nanowire/Graphene and Graphene Asymmetric Electrochemical Capacitors," *ACS Nano* **4**, 5835 (2010).
51. G. Yang and S.-J. Park, "MnO2 and biomass-derived 3D porous carbon composites electrodes for high performance supercapacitor applications," *J. Alloys Compd.*, **741**, 360 (2018).
52. C. Tanggarnjanavalukul, N. Phattharasupakun, J. Wutthiprom, P. Kidkhunthod, and M. Sawangphruk, "Charge storage mechanisms of birnessite-type MnO2 nanosheets in Na2SO4 electrolytes with different pH values: In situ electrochemical X-ray absorption spectroscopy investigation," *Electrochim. Acta.*, **273**, 17 (2018).
53. X. Zhu, P. Zhang, S. Xu, X. Yan, and Q. Xue, "Free-Standing Three-Dimensional Graphene / Manganese Oxide Hybrids As Binder-Free Electrode Materials for Energy Storage Applications" *ACS Appl. Mater. Interfaces., 6, 11665* (2014).
54. A. Viswanathan and A. N. Shetty, "Facile in-situ single step chemical synthesis of reduced graphene oxide-copper oxide-polyaniline nanocomposite and its electrochemical performance for supercapacitor application," *Electrochim. Acta.*, **257**, 483 (2017).
55. L. Xu, L. Sun, J. Feng, L. Qi, I. Muhammad, J. Maher, X. Cheng, and W. Song, "Nanocasting synthesis of an iron nitride-ordered mesopore carbon composite as a novel electrode material for supercapacitors," *RSC Advances* **7**, 44619 (2017).
56. W. Liu, C. Lu, X. Wang, R. Y. Tay, and B. K. Tay, "High-Performance Microsupercapacitors Based on Two-Dimensional Graphene/Manganese Dioxide/Silver Nanowire Ternary Hybrid Film," *ACS Nano* **9**, 1528 (2015).
57. G. P. Awasthi, D. Kumar, B. K. Shrestha, J. Kim, K.-S. Kim, C. H. Park, and C. S. Kim, "Layer – Structured partially reduced graphene oxide sheathed mesoporous MoS2 particles for energy storage applications," *J. Colloid Interface Sci.*, **518**, 234 (2018)..